Computational Materials Science 83 (2014) 196–206

Contents lists available at ScienceDirect

Computational Materials Science

journal homepage: www.elsevier.com/locate/commatsci

Molecular dynamics simulations of influence of Re on lattice trapping and fracture stress of cracks in Ni

Zheng-Guang Liu [a,d], Chong-Yu Wang [a,b,c,*], Tao Yu [a]

[a] Central Iron and Steel Research Institute, Beijing 100081, China
[b] Department of Physics, Tsinghua University, Beijing 100084, China
[c] International Centre for Materials Physics, Academia Sinica, Shenyang 110016, China
[d] Department of Physics, North University of China, Taiyuan 030051, China

ARTICLE INFO

Article history:
Received 24 August 2013
Received in revised form 19 October 2013
Accepted 5 November 2013

Keywords:
Fracture
Lattice trapping
Molecular dynamics
Ni (Re) solid solution

ABSTRACT

The influence of Re on the lattice trapping and fracture stress of the five orientation cracks in Ni was investigated using the molecular dynamics (MD) method, with a Ni–Al–Re embedded-atom-method potential. The MD simulations showed that the range (S) of lattice trapping for different crack orientations was small, regardless of the addition of Re. With the addition of 3 at.% or 6 at.% Re, the lower and upper trapping limits ($K_{IC}^{\pm}$) increased noticeably and exceeded the theoretical Griffith load. This means that Re–Ni interatomic interactions can prevent the breaking of atomic bonds and can heal cracks. With the addition of Re, the largest and smallest fracture stresses occurred in the (010)[101] and (100)[010] crack systems, respectively. The MD simulations also showed that in dilute and concentrated Ni (Re) solid solutions, the ranges (R) over which Re atoms restrained the jumps in the bond lengths of atom pairs in neighbouring regions were different. R was proportional to $K_{IC}^{\pm}$. In addition, kinks in crack fronts were found not to affect S and R.

1. Introduction

Final rupture is often displayed by cracks in materials. The fracture stress is closely connected to the critical activation of crack, which is closely related to the lattice trapping of the crack. As a result of lattice trapping of cracks, which was first described by Thomson et al. [1], cracks remain stable and do not advance or heal until the load is larger or smaller than the Griffith load. The critical loads for a crack to advance or heal are called the upper and lower trapping limits, respectively. To determine the fracture stress accurately, the lattice trapping of a crack needs to be investigated.

In macroscopic experiments, the lattice trapping of cracks in face-centred cubic (fcc) Ni is difficult to study. The metal does not often show large trapping effects and is not brittle enough to be well studied experimentally [2]. However, brittle cracks can occur for specific crack systems in crystalline Ni [3,4]. In particular, doping of Ni with a heavy element such as Re could result in Ni–Re interatomic interactions that might result in a large lattice-trapping effect (or at least increase the upper trapping limit). Stronger atomic bonding between solute and matrix atoms is likely to improve the fracture stress. It is therefore useful to explore the influence of Re on lattice trapping of cracks in Ni.

Lattice trapping can easily be studied theoretically on the atomic scale using the molecular dynamics (MD) method. In MD simulations, the range of the lattice trapping strongly depends on the interatomic potentials. Some studies [2,5,6] have shown that for long-range interatomic potentials, the lattice trapping of bond breaking at the crack tip is small. Using various simplified interatomic force laws, Zhu et al. [7] found that a steep slope on the back side of the force law will lead to a large lattice-trapping range for the brittle fracture in Si. Based on an embedded-atom-method (EAM) potential, Gumbsch [3] showed a small lattice-trapping effect for a close-packed lattice and "soft" interatomic interaction model about the crack propagation in Ni. Using a one-dimensional lattice model, Fuller and Thomson [8] pointed out that "stiffer" bendable spring elements and/or "softer" stretchable spring elements result in a decrease in the lattice-trapping regime. Schoeck and Pichl [9] showed that the magnitude of the trapping mainly depends on the relative stiffness of the crack-tip bond compared with the combined stiffness of all the bonds that load the crack-tip atoms. Pérez and Gumbsch [10] found that the atomic rearrangements and relaxations in the immediate neighbourhood of the crack tip in Si can be responsible for the large trapping range.

There may be other factors that can affect the trapping range, especially in solid solutions. The range over which solute atoms can affect the bond breaking of atoms in the local region is an

* Corresponding author at: Department of Physics, Tsinghua University, Beijing 100084, China. Tel.: +86 01062772782.
E-mail addresses: guang212@163.com (Z.-G. Liu), cywang@mail.tsinghua.edu.cn (C.-Y. Wang), ytao012345@163.com (T. Yu).

0927-0256/$ - see front matter © 2013 Elsevier B.V. All rights reserved.
http://dx.doi.org/10.1016/j.commatsci.2013.11.008

interesting factor. It is assumed that the upper trapping limits will be improved if the range is large. Kinks in the crack front are another factor. If a kink appears, the activation energy for crack advance is small, and the trapping range should be small [5,7]. These factors need to be explored.

In the present work, the influence of Re on the lattice trapping and fracture stress of the brittle cracks in Ni was investigated at 5 K, using the MD method with a Ni–Al–Re EAM potential [11]. Based on the MD results, the range (R) over which Re affects the jumps in bond lengths in neighbouring regions, the influence of Re on the range (S) of lattice trapping, the influence of Re on kinks and dislocations at crack tips, and the fracture stress are discussed. The relations among S, R, and kink are analysed.

2. Model and procedures

2.1. Model of crack

In the present work, an atomistic sharp crack in a Ni matrix was initially constructed using the anisotropic linear elastic continuum solution [12] with a stress intensity factor K_I. A mode I (tensile) crack was considered. Five different crack orientations, namely $(1\,1\,1)[\bar{1}\,\bar{1}\,2]$, $(0\,1\,0)[1\,0\,1]$, $(1\,0\,0)[0\,1\,0]$, $(0\,\bar{1}\,1)[1\,0\,0]$, and $(\bar{1}\,1\,0)[\bar{1}\,\bar{1}\,2]$, were analysed. As an example, the $(0\,1\,0)[1\,0\,1]$ crack system is shown in Fig. 1. The crack surface was a $(0\,1\,0)$ plane, and the crack front was oriented along the $[1\,0\,1]$ direction. The simulated system consisted of 112 atomic layers in the x $[1\,0\,\bar{1}]$ direction, 120 atomic layers in the y $[0\,1\,0]$ direction, and 160 atomic layers in the z $[1\,0\,1]$ direction. The total number of atoms in the system was 537600. The initial crack length was about $a = 40$ Å.

2.2. The evaluation of lower and upper trapping limits

After determining the initial configurations of the crack at different loads, K_I, the atoms at the crack tip were fully relaxed, with the fixed-displacement boundary condition (the outermost four layers of atoms in the x $[1\,0\,\bar{1}]$ and y $[0\,1\,0]$ directions were both fixed). The loading or unloading scheme has been described in the literature [10]. The loading or unloading was started at a stress intensity that fulfilled the Griffith criterion (crack systems are stable at this load, which means that the crack tip does not advance or recede), and the relaxed structures were then taken as the starting points for further loading or unloading by proportional scaling of the boundary displacements. The loading or unloading was performed in increments of 1% of the Griffith load. The lower trapping limit (K_{IC}^-) and upper trapping limit (K_{IC}^+) were then determined according to the sudden decrease and increase, respectively, in the average bond length at the crack tip.

The average bond length at the crack tip can be expressed as follows:

$$d_{ij} = \frac{1}{n}\sum_{k=1}^{n} l_{ijk} \tag{1}$$

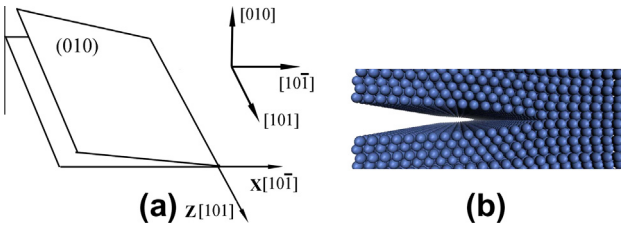

Fig. 1. (a) Sketch map of atomically sharp $(0\,1\,0)[1\,0\,1]$ crack and (b) atomic configuration of side view for $(0\,1\,0)[1\,0\,1]$ crack tip.

where d_{ij} is the average bond length of atom pairs between atomic row i (in the upper crack surface) and atomic row j (in the lower crack surface), and n is the total number of atoms in atomic row i or j. Fig. 2 shows the atomic configurations of the eight atomic rows ($i, j = 1, 2, 3, 4$) at the $(0\,1\,0)[1\,0\,1]$ crack tip. In Fig. 2, there are seven average bond lengths (d_{11}, d_{21}, d_{22}, d_{32}, d_{33}, d_{43}, d_{44}) between the eight atomic rows. l_{ijk} is the bond length of the atom pair consisting of atom k (in atomic row i of the upper crack surface) and atom k (in atomic row j of the lower crack surface). In the present work, it was judged that the bonds were stable (neither broken nor healed) when $d_{ij} \approx 2.65 - 3.2$ Å, and based on observation of the atomic configuration of the crack tip in the MD simulation. When $d_{ij} \geqslant 3.3$ Å, the crack tip was taken as advancing (the value of 3.3 Å is consistent with the value of the crack formation length (l_f) calculated using the MD method, and l_f can be obtained by fitting the relation between the decohesion energy and opening distance [13]). K_{IC}^- or K_{IC}^+ is often obtained using the athermal limit of K_I, at which the activation energy barrier (for bond healing or breaking at the crack tip) vanishes [6,7,14]. However, it is difficult to obtain the activation energy barrier in Ni. The initial and final local equilibrium states (before and after the bond heals or breaks) are difficult to obtained because of the very small activation energy barrier in Ni. We tried to determine the initial and final states, but have failed so far, even when Re was added to the crack system. In the present work, $K_{IC}^{\pm}$ values were therefore determined based on sudden jumps in the average bond length, as described in the literature [10,15].

After obtaining K_{IC}^- and K_{IC}^+, the lattice-trapping range can be evaluated from [10]

$$S \equiv K_{IC}^+/K_{IC}^- - 1 \tag{2}$$

In the MD simulations, the periodic boundary condition was used in the z $[1\,0\,1]$ direction. Newton's equations of motion in the MD were solved using the Gear Algorithm [16]. A time step of 5×10^{-15} s was used. The temperature of the system remained at 5 K throughout the simulation, obtained by scaling the instantaneous velocities of all atoms with the appropriate Maxwell–Boltzmann distribution at a specified temperature. The XMD program [17] was used for the atomistic simulations.

The MD simulations at 5 K have some advantages. Comparing with the MD simulations at 0 K, the MD simulations at 5 K can speed, though the results of simulations are similar at 5 K and 0 K; comparing with the molecular statics simulations, the MD simulations at 5 K can give the detailed evolution of defects (for example, the dislocation or kink nucleation).

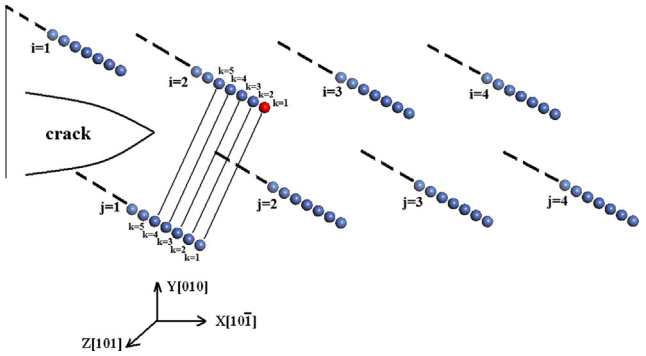

Fig. 2. Atomic configurations of eight atomic rows ($i, j = 1, 2, 3, 4$) at the $(0\,1\,0)[1\,0\,1]$ crack tip, with a single Re atom at the crack front. Black lines represent the bond lengths (l_{211}, l_{212}, l_{213}, l_{214}, and l_{215}) of consecutive five-atom pairs between the atomic rows $i = 2$ and $j = 1$. Blue and red balls represent Ni and Re atoms, respectively. (For interpretation of the references to colour in this figure legend, the reader is referred to the web version of this article.)

To probe the influence of Re on the lattice trapping of a crack, two schemes with Re addition were used in the present work. In the first scheme, a single Re atom was placed at crack front to explore the effect of Re in dilute Ni (Re) solid solution. In the second scheme, 3 at.% or 6 at.% Re was randomly doped into the entire crack system to explore the effect of Re in concentrated Ni (Re) solid solution. In the analysis presented below, only the calculated results of one sample for 3 and 6 at.% Re random distributions are given, but this has no influence on the discussion.

2.3. Ni–Al–Re embedded atom method (EAM) potential

In the present work, the Ni–Al–Re embedded atom method (EAM) potential is used [11]. In the scheme of the EAM [18,19], the embedding energy based on the electron density of atom is also considered, besides the pair-potential between atoms.

The Ni–Al–Re potential fitted the lattice parameters, cohesive energies, vacancy formation energies, and elastic constants of Ni, Al, Re, and their compounds, based on the experimental or first-principle results. Especially, the planar fault energies of Ni and Ni_3Al are in a reasonable agreement with experimental data. The structures of $L1_2$-Ni_3Re, $D0_{19}$-Ni_3Re, $D0_{22}$-Ni_3Re, $L1_2$-Re_3Al, $L1_2$-Al_3Re, B_2-NiRe, B_2-AlRe, and $L2_1$-Ni_2ReAl have been considered when fitting the lattice constants and the binding energies based on the first-principles data. This potential has been applied to predict the effect of Re on the dislocation and crack in Ni/Ni_3Al interface [11,20]. In the present work, this potential is applied to explore the effect of Re on the lattice trapping and fracture stress of the brittle cracks in Ni.

2.4. The properties of Ni

In the MD simulations of crack, some properties (the lattice constant a_0, the compliance matrix A, and the plane strain compliance matrix β) of FCC Ni are often used. In the present work, a_0, A, and β are obtained by the atomic potential. $a_0 = 3.52$ Å is obtained according to the equilibrium structure by the atomic potential, and this value is consistent with the experimental value [21]; A is derived from the second derivative of the potential energy versus the lattice constant; β are obtained by the transformation from A.

When the coordinate axes are along the x [100], y [010], and z [001] directions, A and β are

$$A = \begin{bmatrix} 8.215 & -3.175 & -3.175 & 0 & 0 & 0 \\ -3.175 & 8.215 & -3.175 & 0 & 0 & 0 \\ -3.175 & -3.175 & 8.215 & 0 & 0 & 0 \\ 0 & 0 & 0 & 7.880 & 0 & 0 \\ 0 & 0 & 0 & 0 & 7.880 & 0 \\ 0 & 0 & 0 & 0 & 0 & 7.880 \end{bmatrix} \times 10^{-12} Pa^{-1};$$

$$\beta = \begin{bmatrix} 6.987 & -4.402 & -3.175 & 0 & 0 & 0 \\ -4.402 & 6.987 & -3.175 & 0 & 0 & 0 \\ -3.175 & -3.175 & 8.215 & 0 & 0 & 0 \\ 0 & 0 & 0 & 7.880 & 0 & 0 \\ 0 & 0 & 0 & 0 & 7.880 & 0 \\ 0 & 0 & 0 & 0 & 0 & 7.880 \end{bmatrix} \times 10^{-12} Pa^{-1}.$$

The matrix element β_{ij} of β can be obtained according to the following equation [22]:

$$\beta_{ij} = a_{ij} - \frac{a_{i3}a_{j3}}{a_{33}}, (i, j = 1, 2, 4, 5, 6), \quad (3)$$

where a_{ij} is the matrix element of A. When i or $j = 3$, $\beta_{ij} = a_{ij}$.

When the coordinate axes are along other directions (for example, $x'[10\bar{1}]$, y' [010], and z' [101]), A can be obtained by the coordinate transformation from the x [100], y [010], and z [001] directions. Then, β can be obtained by Eq. (3). As an example, A and β along the $x'[10\bar{1}]$, y' [010], and z' [101] directions are

$$A = \begin{bmatrix} 4.490 & -3.175 & 0.550 & 0 & 0 & 0 \\ -3.175 & 8.215 & -3.175 & 0 & 0 & 0 \\ 0.550 & -3.175 & 4.490 & 0 & 0 & 0 \\ 0 & 0 & 0 & 7.880 & 0 & 0 \\ 0 & 0 & 0 & 0 & 22.780 & 0 \\ 0 & 0 & 0 & 0 & 0 & 7.880 \end{bmatrix} \times 10^{-12} Pa^{-1};$$

$$\beta = \begin{bmatrix} 4.423 & -2.786 & 0.550 & 0 & 0 & 0 \\ -2.786 & 5.970 & -3.175 & 0 & 0 & 0 \\ 0.550 & -3.175 & 4.490 & 0 & 0 & 0 \\ 0 & 0 & 0 & 7.880 & 0 & 0 \\ 0 & 0 & 0 & 0 & 22.780 & 0 \\ 0 & 0 & 0 & 0 & 0 & 7.880 \end{bmatrix} \times 10^{-12} Pa^{-1}.$$

3. Results and discussion

3.1. The bonding strength between Ni and Re atoms

When Re is doped in Ni matrix, the bonding strength between Ni and Re atoms may be stronger than that between Ni and Ni atoms. The stronger Ni–Re interatomic interaction is likely to lead to a large upper lattice-trapping limit, promote the kink nucleation at crack front, and improve the fracture stress. It is instructive to evaluate and compare the Re–Ni and Ni–Ni bonding strengths.

The bonding strength between the solute and the matrix atom can be roughly estimated from the well depth of the pair potential in the EAM potential [23]; in our previous work, the interatomic interaction of Re–Ni has been reported to be stronger than that of Ni–Ni [20]. Here, to test whether the Re–Ni bond is stronger than the Ni–Ni bond in a Ni matrix, the bond strength is also evaluated from the interatomic energy (IE) [24,25], using an ab initio calculation. The IE is a local quantity that can be used to evaluate the bonding strength of atoms in the local region.

The IE between atom l and atom m, E_{lm}, is defined as

$$E_{lm} = \sum_n \sum_{\alpha\beta} N_n a^*_{n\alpha l} a_{n\beta m} H_{\beta m \alpha l} \quad (4)$$

where N_n is the electron occupation number for the molecular orbital ψ_n, $a_{n\alpha l} = \langle \phi_{\alpha l} | \psi_n(r) \rangle$, and $H_{\beta m \alpha l}$ is the Hamiltonian matrix element connecting the atomic orbital β of atom m to the atomic orbital α of atom l. The IE can be used to evaluate the bonding strengths of two atoms since it is related to the Hamiltonian matrix element. Usually, a negative IE with a large absolute value means a strong interatomic interaction. The IE can be calculated using the discrete-variational method (DVM) [26]. The DVM is a first-principles numerical method for solving local-density-functional equations, and has been used successfully to study the electronic structures of metals and alloys [26,27].

In the calculation of the IE, a computational supercell ($3 \times 3 \times 3$) with 108 atoms containing a Re atom is adopted (Fig. 4). First, the supercell is relaxed to an equilibrium configuration with periodic boundary conditions in the x, y, and z directions, using the plane-wave basis VASP code [28,29]. Then, the average value of the interatomic energies between Re and the 12 first-neighbour atoms is calculated using the DVM code.

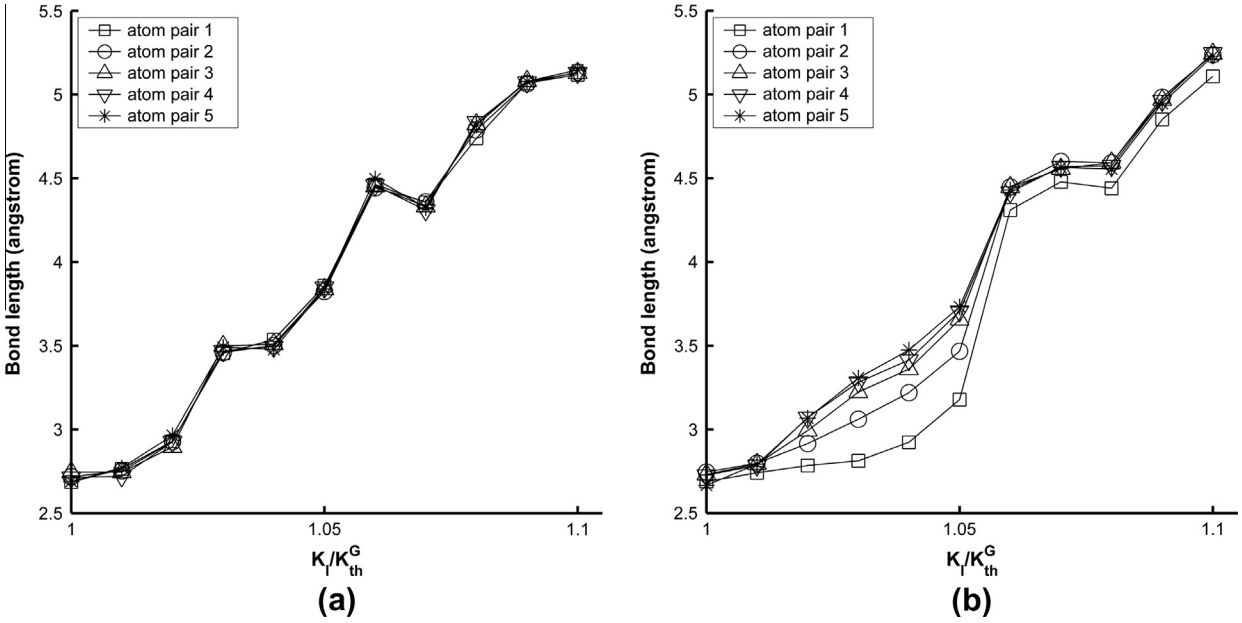

Fig. 3. Variations in lengths of five consecutive bonds (at the (010)[101] crack front) with loading stress intensity factor. Bond lengths of atom pairs 1, 2, 3, 4, and 5 are represented by l_{211}, l_{212}, l_{213}, l_{214}, and l_{215} (defined in Eq. (1)), respectively: (a) without Re atom at the crack front and (b) with a single Re atom at the crack front. Atom pair 1 represents the Re–Ni atom pair.

Spin-polarization is performed considering the magnetic effects. The IE results show that the average value of the interatomic energies of Re–Ni is −1.34 eV, and that of Ni–Ni is −0.18 eV. On addition of Re, the absolute value of IE increases by 644%. This means that the interatomic interaction of Re–Ni is indeed stronger than that of Ni–Ni.

3.2. Influence of single Re on lattice trapping of crack

In this section, three points are discussed. The first point is the range (R) over which a single Re atom can affect the jump in bond length in the neighbouring region (of the Re atom) along the crack front. The second point is the influence of a single Re atom on the lattice-trapping range. The third point is whether a kink forms at the crack front.

To explore the three points, a single Re atom is put at the crack front. Fig. 2 shows the position of the Re atom at the (010)[101] crack tip. In Fig. 2, five consecutive bonds (k = 1, 2, 3, 4, and 5) at the crack front are depicted; the Re–Ni bond has k = 1.

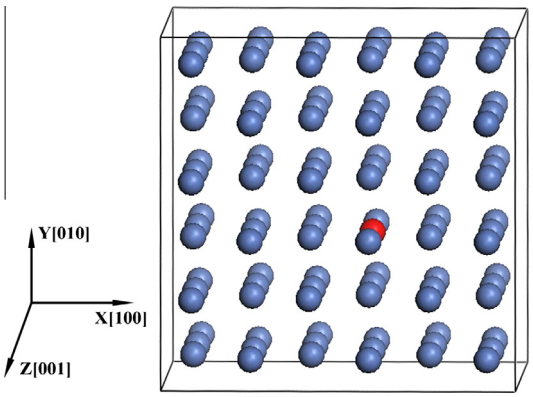

Fig. 4. Computational supercell (3 × 3 × 3) of IE in fcc Ni. Red and blue balls represent Re and Ni atoms, respectively. (For interpretation of the references to colour in this figure legend, the reader is referred to the web version of this article.)

3.2.1. Range over which single Re atom affects jump in bond length

R is an interesting parameter. It is assumed that K_{IC}^{+} improves if R is large, and a kink at the crack front easily forms. R may be different in dilute and concentrated Ni (Re) solid solutions. In this section, R is explored for a dilute Ni (Re) solid solution.

Fig. 3 shows the variations in the lengths of the five consecutive bonds at the (010)[101] crack front with the loading stress intensity factor, without or with a single Re atom at the crack front. From Fig. 3(b), it can be seen that the jumps in the bond lengths of atom pairs 1 and 2 (l_{211} and l_{212}) are restrained during the loading process. This means that the jumps in the bond lengths of atom pairs (near the Re atom) are restrained, and the Re–Ni interatomic interaction is stronger than the Ni–Ni interaction. Beyond the distance R between the atoms k = 1 and k = 2 (namely the distance from the Re atom to the first-neighbour atom at the crack front), the jump in the bond length at the crack front is not influenced. Thus, $R = 1 \times (\sqrt{2}/2)a_0 \approx 2.49$ Å for the (010)[101] crack system.

The MD simulations show that of the five crack orientations, only the jump in bond length of the first-neighbour atom (at the crack front) of the Re atom is influenced. So, for the five crack orientations, $R < 4.5$ Å (the calculated results for R are listed in Table 1).

3.2.2. Influence of single Re atom on lattice-trapping range

In this section, the influence of a single Re atom on both K_{IC}^{+} and K_{IC}^{-} for the entire crack system is explored.

Fig. 5 shows the variations in the seven average bond lengths at the (010)[101] crack tip with the loading stress intensity factor, without or with a single Re atom at the crack front. A comparison of Fig. 5(a) and (b) shows that a jump in the average bond length does not occur at larger K_I values, and the curves even become smoother. At $K_I/K_{th}^{G} = 1.01$, there is a slight jump in the curves in both Fig. 5(a) and (b). When $K_I/K_{th}^{G} > 1.01$, both d_{11} and d_{21} clearly increase, and the crack tips advance. Thus, $K_{IC}^{+} = 1.01$, whether or not a single Re atom is added at the crack front.

The MD simulation shows that the K_{IC}^{-} value for the entire crack system is unchanged by the addition of a single Re atom. Fig. 6 shows the variations in the average bond lengths at the

Table 1
Lower and upper trapping limits (K_{IC}^{-} and K_{IC}^{+}); the range (R) over which a single Re atom can affect the jump in bond length in the neighbouring region (of the Re atom) along the crack front.

Crack orientation	Dimension	Without Re		1 Re atom			3 at.% Re		6 at.% Re	
		$\frac{K_{IC}^{-}}{K_{th}^{G}}$	$\frac{K_{IC}^{+}}{K_{th}^{G}}$	$\frac{K_{IC}^{-}}{K_{th}^{G}}$	$\frac{K_{IC}^{+}}{K_{th}^{G}}$	R(Å)	$\frac{K_{IC}^{-}}{K_{th}^{G}}$	$\frac{K_{IC}^{+}}{K_{th}^{G}}$	$\frac{K_{IC}^{-}}{K_{th}^{G}}$	$\frac{K_{IC}^{+}}{K_{th}^{G}}$
(010)[101]	$28\sqrt{2}\times 60\times 20\sqrt{2}$	0.99	1.01	0.99	1.02	2.49	1.12	1.15	1.25	1.28
	$28\sqrt{2}\times 60\times 40\sqrt{2}$	0.99	1.01	0.99	1.01	2.49	1.11	1.14	1.26	1.29
(111)[$\bar{1}\bar{1}$2]	$30\sqrt{2}\times 30\sqrt{3}\times 24\sqrt{6}/2$	0.99	1.01	0.99	1.02	4.31	D	D	D	D
	$30\sqrt{2}\times 30\sqrt{3}\times 48\sqrt{6}/2$	1.00	1.02	0.99	1.02	4.31	D	D	D	D
(100)[010]	$40\times 60\times 30$	0.98	1.01	0.99	1.03	3.52	1.14	1.17	1.24	1.26
	$40\times 60\times 60$	0.99	1.01	0.99	1.01	3.52	1.14	1.16	1.26	1.29
(0$\bar{1}$1)[100]	$30\sqrt{2}\times 30\sqrt{2}\times 30$	0.99	1.01	1.00	1.02	3.52	1.14	1.18	D	D
	$30\sqrt{2}\times 30\sqrt{2}\times 60$	1.00	1.02	1.00	1.02	3.52	1.13	1.16	D	D
($\bar{1}$10)[$\bar{1}\bar{1}$2]	$30\sqrt{3}\times 30\sqrt{2}\times 24\sqrt{6}/2$	0.99	1.01	1.00	1.02	4.31	D	D	D	D
	$30\sqrt{3}\times 30\sqrt{2}\times 48\sqrt{6}/2$	0.99	1.01	0.99	1.01	4.31	D	D	D	D

Note: "D" indicates that the dislocation emission takes place at the crack tip. K_{th}^{G} is the theoretical Griffith stress intensity factor.

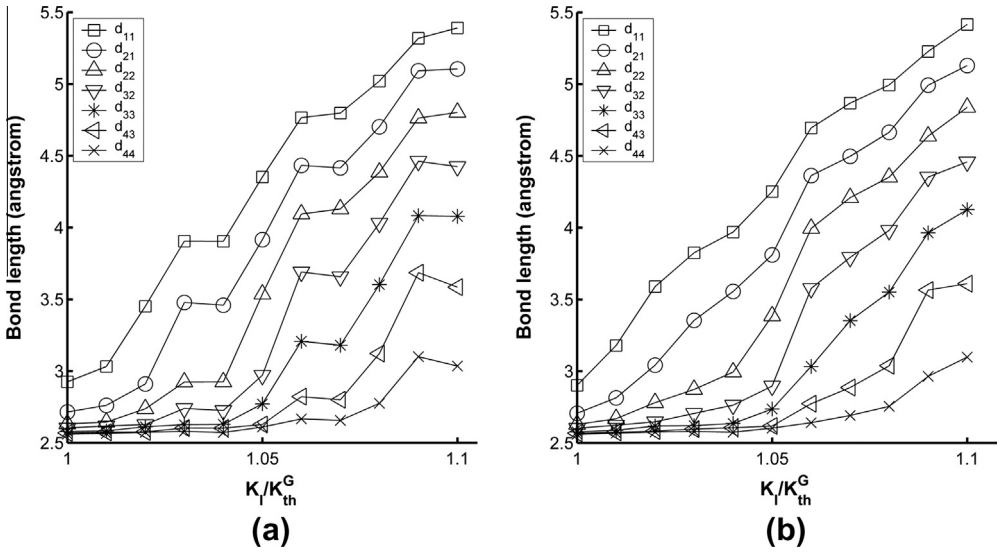

Fig. 5. Variations in seven average bond lengths (d_{11}, d_{21}, d_{22}, d_{32}, d_{33}, d_{43}, d_{44}, defined in Eq. (1)) at the (010)[101] crack tip with loading stress intensity factor: (a) without a single Re atom at the crack front and (b) with a single Re atom at the crack front.

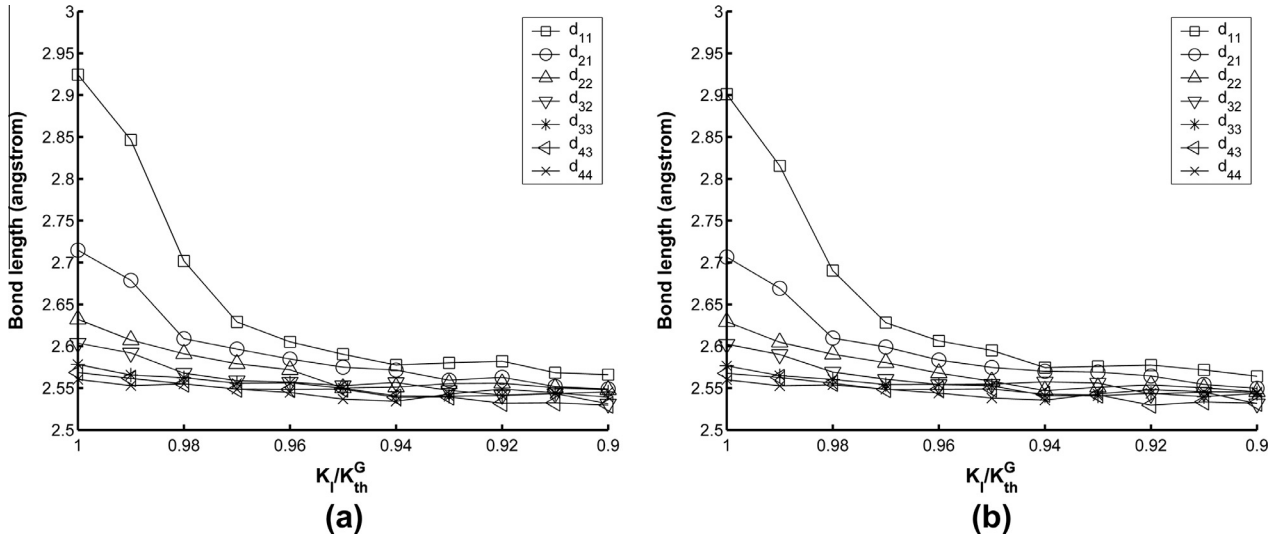

Fig. 6. Variations in average bond lengths at the (010)[101] crack tip with unloading stress intensity factor (a) without a single Re atom at the crack front and (b) with a single Re atom at the crack front.

(0 1 0)[1 0 1] crack tip with unloading stress intensity factor, without or with a single Re atom at the crack front. A comparison of Fig. 6(a) and (b) shows that the curves are almost the same, and there is a slight jump in the curves at $K_I/K_{th}^G = 0.99$. When $K_I/K_{th}^G < 0.99$, d_{11} and d_{21} clearly decrease, and the crack tips heal. Thus, $K_{IC}^- = 0.99$, whether or not a single Re atom is added at the crack front.

It is noticed in the present work that the breaking or healing of atomic bonds (in the consecutive atomic rows at the crack tip) take place simultaneously. This may be caused by the long-range character of interatomic interactions in metals. This case is different from that for Si [7,10]. In Si, the breaking or healing of each atomic bond can take place independently at the crack tip. In Ni, the breaking or healing of atomic bonds should be judged based on the observations for the several consecutive atomic rows at crack tip.

The calculated K_{IC}^- and K_{IC}^+ values are listed in Table 1. The data in Table 1 show that a single Re atom does not affect K_{IC}^+ and K_{IC}^- in the entire crack system. For the five different crack orientations, $K_{IC}^-/K_{th}^G \approx 0.98 \sim 1.00$ and $K_{IC}^+/K_{th}^G \approx 1.01 \sim 1.02$, whether or not a single Re atom is added to the crack system. The lattice-trapping range (S) is therefore estimated to be 0.02–0.04.

It has been pointed out in the literature [6] that for long-range interatomic potentials, the lattice trapping of bond breaking at the crack tip is negligible, and the theoretical Griffith load (K_{th}^G) is a fairly accurate onset condition for crack extension. We have also found that the true Griffith load (K_I^G) in the MD simulation is very close to K_{th}^G, without or with single Re addition.

3.2.3. Influence of single Re on kinks

Kink formation at the crack front in Ni is an issue. Kink formation should be difficult in fcc metals because of their delocalized metallic bonding nature. However, with the addition of Re, we find that kink pairs can form in several crack orientations in Ni.

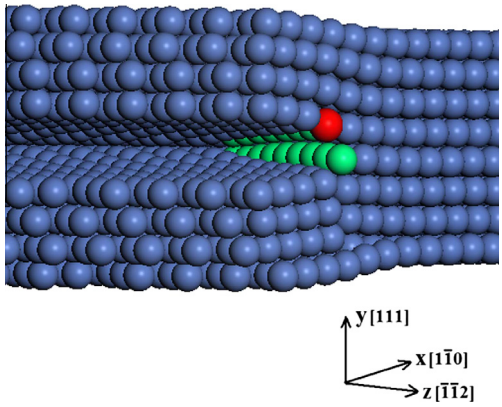

Fig. 8. Atomic configuration of the $(1\,1\,1)[\bar{1}\,\bar{1}\,2]$ crack tip at $K_I/K_{th}^G = 1.11$, with a single Re atom at the crack front. There is a step (depicted by green balls) near the Re atom at the crack front. Blue, green, and red balls represent Ni, Ni, and Re atoms, respectively. (For interpretation of the references to colour in this figure legend, the reader is referred to the web version of this article.)

The simulations find that in the $(1\,1\,1)[\bar{1}\,\bar{1}\,2]$, $(0\,\bar{1}\,1)[1\,0\,0]$, and $(\bar{1}\,1\,0)[\bar{1}\,\bar{1}\,2]$ crack systems, kink pairs appear near the single Re atom. Fig. 7 shows the contour maps of bond lengths for every atom pair across the $(1\,1\,1)[\bar{1}\,\bar{1}\,2]$ crack surface during the loading process, with a single Re atom at the crack front. In Fig. 7, a sharp kink pair appears near the Re atom. Fig. 8 shows the atomic configuration of the $(1\,1\,1)[\bar{1}\,\bar{1}\,2]$ crack tip at $K_I/K_{th}^G = 1.11$, with a single Re atom at the crack front. In Fig. 8, a step kink near the Re atom forms at the crack front, and the width of the kink is about $8(\sqrt{6}/4)a_0 = 17.24$ Å. The formation of kink pair is due to the stronger pinning of Re at the crack front.

In the (0 1 0)[1 0 1] and (1 0 0)[0 1 0] crack systems, kink pairs are not found near the Re atom. Fig. 9 shows the atomic configuration

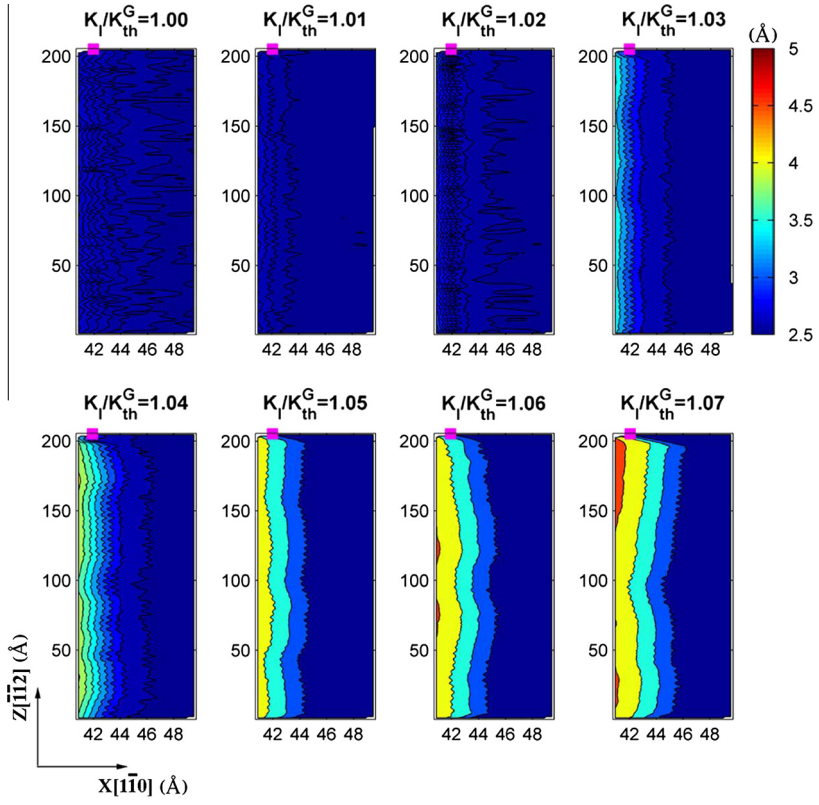

Fig. 7. Contour maps of bond lengths for every atom pair across the $(1\,1\,1)[\bar{1}\,\bar{1}\,2]$ crack surface during the loading process, with a single Re atom at the crack front. The pink square in the top left corner represents the position of the Re atom. (For interpretation of the references to colour in this figure legend, the reader is referred to the web version of this article.)

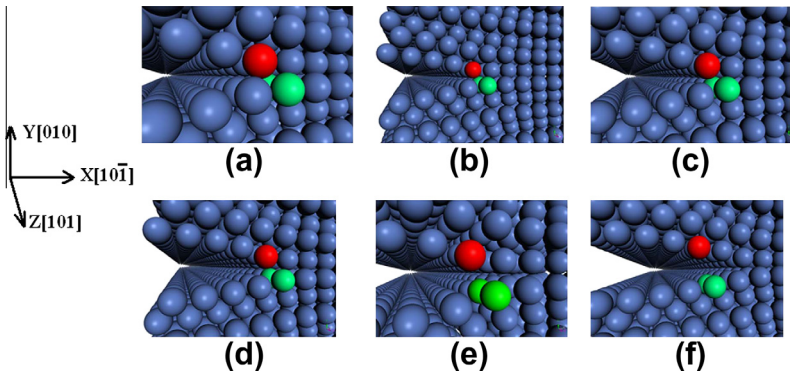

Fig. 9. Atomic configurations of the (0 1 0)[1 0 1] crack tip with a single Re atom at the crack front at (a) $K_I/K_{th}^G = 1.00$, (b) $K_I/K_{th}^G = 1.01$, (c) $K_I/K_{th}^G = 1.02$, (d) $K_I/K_{th}^G = 1.04$, (e) $K_I/K_{th}^G = 1.05$, and (f) $K_I/K_{th}^G = 1.06$. Blue, green, and red balls represent Ni, Ni, and Re atoms, respectively. A slight kink structure occurs near the two green Ni atoms. (For interpretation of the references to colour in this figure legend, the reader is referred to the web version of this article.)

of the (0 1 0)[1 0 1] crack tip during the loading process, with a single Re atom at the crack front. In Fig. 9, the crack front is almost a straight line, and only a slight kink occurs near the Re atom. The slight kink occurs because of the attraction between the Re atom (in the upper crack surface) and the two Ni atoms (in the lower crack surface).

The reason that the kink pairs appear in (1 1 1)[$\bar{1}\,\bar{1}$ 2], (0 $\bar{1}$ 1)[1 0 0], and ($\bar{1}$ 1 0)[$\bar{1}\,\bar{1}$ 2] crack systems (not in (0 1 0)[1 0 1] and (1 0 0)[0 1 0] crack systems) with the addition of Re has not been found by us, however, this should not be owed to the surface energy difference in the different crack systems. The surface energies for the {1 1 1}, {1 0 0}, and {1 1 0} planes (without or with a single Re atom addition) are 1.4993 J/m^2, 1.5924 J/m^2, and 1.6941 J/m^2 in the present MD simulations. The crack surfaces in the (0 1 0)[1 0 1] and (1 0 0)[0 1 0] crack systems belong to the {1 0 0} planes whose surface energies are smaller and larger than that of {1 1 1} and {1 1 0} planes, respectively. And the {1 1 1} and {1 1 0} planes are the crack surfaces in the (1 1 1)[$\bar{1}\,\bar{1}$ 2], (0 $\bar{1}$ 1)[1 0 0] and ($\bar{1}$ 1 0)[$\bar{1}\,\bar{1}$ 2] crack systems in which the kink pairs appear. Thus, the appearance of kink pairs should not be owed to the surface energy difference in the different crack systems.

It has been explained in the literature [10] that the large range of lattice trapping in Si is related to atomic rearrangements and relaxations in the immediate neighbourhood of the crack tip. In the present MD simulations, kink pairs and atomic rearrangements near the Re atom at the crack front are also found in several crack systems. However, the lattice-trapping ranges are still small, and do not change. Local atomic rearrangements in the kinks near the Re atom therefore seem to be unrelated to the lattice-trapping ranges in dilute Ni (Re) solid solutions.

On the other hand, it was conjectured in the literature [5,7] that the trapping range is small if the kink forms at crack front in the system, since the activation energy for crack advance in the kink way is small. This is not in contradiction with the present MD simulations results. Because the system (in which kinks appear with Re addition) is not the same system (in which kinks do not appear without Re addition).

In addition, combining these results with the discussion of R in Section 3.2.1, it can be seen that R is also small and does not change, regardless of whether a kink appears at the crack tip, and the appearance of a kink is irrelevant to R in a dilute Ni (Re) solid solution.

3.3. Influence of Re concentration on lattice trapping and fracture stress

In this section, five points are discussed. The first, second, and third points are R, S, and kink in concentrated Ni (Re) solid solution, respectively. The fourth point is the relation between kink and dislocation at crack tip. The fifth point is the influence of Re concentration on fracture stress.

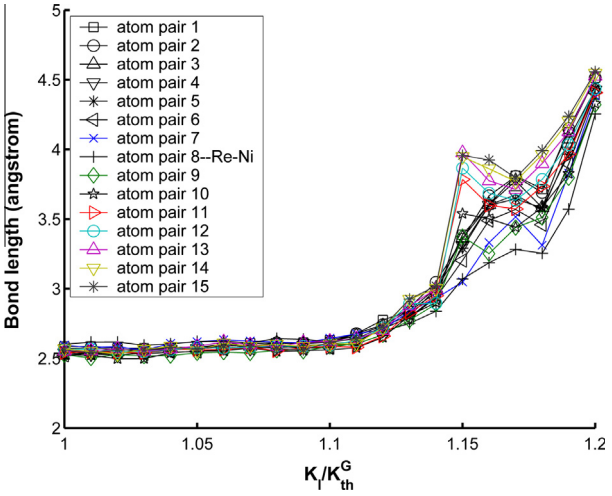

Fig. 10. Variations in lengths of 15 consecutive bonds at the (0 1 0)[1 0 1] crack front with loading stress intensity factors, with 3 at.% Re addition to the crack system. The bond lengths of atom pairs 1, 2, 3, ..., 15 are l_{211}, l_{212}, l_{213}, ..., l_{2115} (defined in Eq. (1)), respectively. Atom pair 8 represents the Re–Ni atom pair, and the other atom pairs represent Ni–Ni atom pairs.

3.3.1. Range of Re atom affecting jump in bond length in concentrated Ni (Re) solid solution

Fig. 10 shows the variations in the lengths of the 15 consecutive bonds at the (0 1 0)[1 0 1] crack front with loading stress intensity factor, with addition of 3 at.% Re to the crack system. From Fig. 10, it can be seen that the jumps in the bond lengths (l_{211}, l_{212}, l_{213}, ..., l_{2115}) of all the atom pairs (1, 2, 3, ..., 15) are restrained until $K_I/K_{th}^G = 1.14$. Thus, $R > [(15-1)/2] \times (\sqrt{2}/2)a_0 = 17.42$ Å for the (0 1 0)[1 0 1] crack system. The MD simulations show that similar cases occur for other crack orientations. This means that R in a concentrated Ni (Re) solid solution is much larger than that in a dilute Ni (Re) solid solution.

3.3.2. Influence of Re concentration on lattice-trapping range

In this section, the influence of 3 at.% or 6 at.% Re on $K_{IC}^{\pm}$ for the entire crack system is explored.

The calculated K_{IC}^- and K_{IC}^+ values are listed in Table 1. From the data in Table 1, it can be seen that both K_{IC}^- and K_{IC}^+ increase significantly as a result of addition of 3 at.% or 6 at.% Re. For the addition

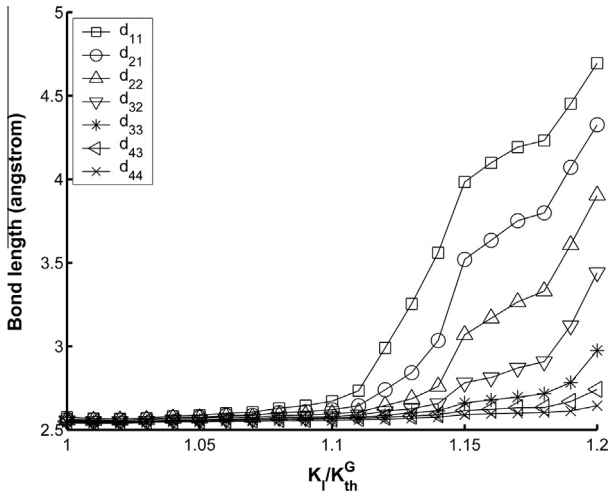

Fig. 11. Variation in seven average bond lengths ($d_{11}, d_{21}, d_{22}, d_{32}, d_{33}, d_{43}, d_{44}$, defined in Eq. (1)) at the (010)[101] crack tip with loading stress intensity factor when 3 at.% Re is added to the system.

of 3 at.% Re, K_{IC}^-/K_{th}^G and K_{IC}^+/K_{th}^G usually lie between 1.10 and 1.20. For the addition of 6 at.% Re, K_{IC}^-/K_{th}^G and K_{IC}^+/K_{th}^G usually lie between 1.20 and 1.30. This means that the Re–Ni atomic interaction can prevent the breaking of atomic bonds and heal the crack. However, the lattice-trapping range is also small ($S = K_{IC}^+/K_{IC}^- - 1 \approx 0.03$), even though 3 at.% or 6 at.% Re is doped into the crack system. This implies that the Re–Ni interatomic interaction is also long range compared with the Ni–Ni interatomic interaction.

As an example, Fig. 11 shows the variations in the average bond length at the (010)[101] crack tip with loading stress intensity factor when 3 at.% Re is added to the system. In Fig. 11, K_{IC}^-/K_{th}^G and K_{IC}^+/K_{th}^G are 1.11 and 1.14, respectively. The lattice-trapping range ($S = K_{IC}^+/K_{IC}^- - 1$) is therefore about 0.03.

Combining the discussions in Sections 3.2.1, 3.2.2, 3.3.1, and 3.3.2, it is seen that both $K_{IC}^{\pm}$ and R are higher in a concentrated Ni (Re) solid solution than in a dilute Ni (Re) solid solution. Thus, $K_{IC}^{\pm}$ is proportional to R.

3.3.3. Influence of Re concentration on kinks

The simulations find that kink pairs appear near the Re atoms in the $(1\,1\,1)[\bar{1}\,\bar{1}\,2]$, $(0\,\bar{1}\,1)[1\,0\,0]$, and $(\bar{1}\,1\,0)[\bar{1}\,\bar{1}\,2]$ crack systems with addition of 3 at.% or 6 at.% Re. Fig. 12 shows the contour maps of bond lengths for every atom pair across the $(0\,\bar{1}\,1)[1\,0\,0]$ crack surface during the loading process, with 3 at.% Re addition. In Fig. 12, kink pairs appear near the Re atoms.

However, kink pairs do not appear in the (010)[101] and (100)[010] crack systems with 3 at.% or 6 at.% Re addition. This may mean that pinning of Re atoms on the advancing crack is weak at the (010)[101] and (100)[010] crack tips, so kink pairs do not appear.

Combining these results with the discussion of S in Section 3.3.2 shows that the appearance of a kink at the crack front does not affect S in a concentrated Ni (Re) solid solution. S is still small and does not change, regardless of whether kinks appear at the crack front. Local atomic rearrangements in the kinks near the Re atom seem not to be related to the lattice-trapping range in a concentrated Ni (Re) solid solution, the same as in a dilute Ni (Re) solid solution, as discussed in Section 3.2.3.

Combining these findings with the discussion of R in Section 3.3.1, it can be seen that the appearance of a kink at the crack front does not affect R in a concentrated Ni (Re) solid solution. Although R increases in a concentrated Ni (Re) solid solution, kinks do not appear in some crack orientations.

3.3.4. Relation between kink and dislocation at crack tip

In the MD simulations, it is found that in the $(1\,1\,1)[\bar{1}\,\bar{1}\,2]$, $(0\,\bar{1}\,1)[1\,0\,0]$, and $(\bar{1}\,1\,0)[\bar{1}\,\bar{1}\,2]$ crack systems at 5 K, dislocations appear near the crack tip during the loading or unloading process,

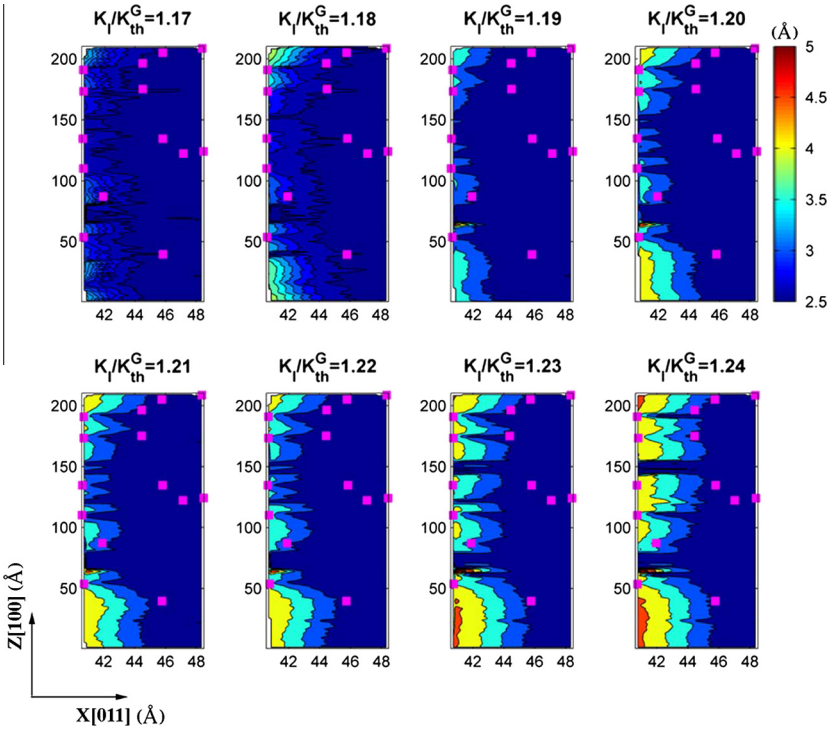

Fig. 12. Contour maps of bond lengths for every atom pair across the $(0\,\bar{1}\,1)[1\,0\,0]$ crack surface during the loading process, with the addition of 3 at.% Re. The pink squares represent the positions of Re atoms. (For interpretation of the references to colour in this figure legend, the reader is referred to the web version of this article.)

Table 2
Appearance or non-appearance of kinks and dislocations for different crack orientations at 5 K.

Crack orientation	Without Re		1 Re atom		3 at.% Re		6 at.% Re	
	Kink	D	Kink	D	Kink	D	Kink	D
(010)[101]	No	No	No	No	No	No	No	No
(111)[$\bar{1}\bar{1}$2]	No	No	Yes	No	Yes	Yes	Yes	Yes
(100)[010]	No	No	No	No	No	No	No	No
(0$\bar{1}$1)[100]	No	No	Yes	No	Yes	No	Yes	Yes
($\bar{1}$10)[$\bar{1}\bar{1}$2]	No	No	Yes	No	Yes	Yes	Yes	Yes

Note: "Kink" indicates that a kink appears at the crack front. "D" shows that dislocation emission takes place at the crack tip.

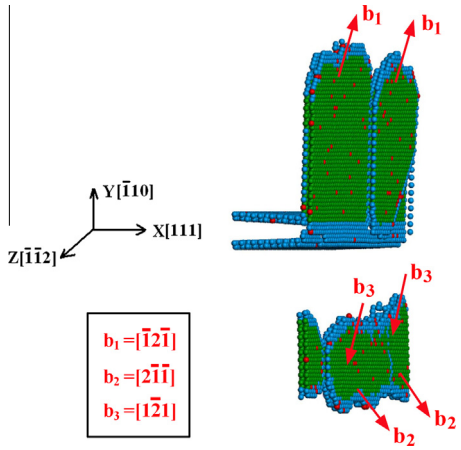

Fig. 13. The partial dislocations emitted from (010)[101] crack tip at 5 K, with $K_I = 1.0K_{th}^G$ and 3 at.% Re addition. The red balls represent Re atoms, and other colour balls represent Ni atoms. The green balls belong to the hexagonal close packed (HCP) structure, ant the atoms belong to FCC structure have been deleted. b_1, b_2, and b_3 represent the Burgers vectors of dislocations in (111) slip plane. (For interpretation of the references to colour in this figure legend, the reader is referred to the web version of this article.)

with addition of 3 at.% or 6 at.% Re. The simulation results are listed in Table 2. In Table 2, the appearance or otherwise of kinks at the crack front is also indicated.

As an example, Fig. 13 shows the dislocations emitted from the ($\bar{1}$10)[$\bar{1}\bar{1}$2] crack tip at $K_I = 1.0K_{th}^G$, with the addition of 3 at.% Re. In Fig. 13, $a_0/6[\bar{1}2\bar{1}](111)$, $a_0/6[2\bar{1}\bar{1}](111)$, and $a_0/6[1\bar{2}1](111)$ partial dislocation loops appear in the multiple (111) layers near the crack tip. For the (111)[$\bar{1}\bar{1}$2] and (0$\bar{1}$1)[100] crack systems at $K_I = 1.0K_{th}^G$ with the addition of 6 at.% Re, $a_0/6[\bar{1}\bar{1}2](11\bar{1})$, $a_0/6[1\bar{1}\bar{2}](\bar{1}1\bar{1})$, and $a_0/6[211](\bar{1}11)$, $a_0/6[\bar{2}11](\bar{1}11)$, $a_0/6[\bar{2}\bar{1}1]$ $(1\bar{1}\bar{1})$ partial dislocation loops are observed in the multiple (111) layers near the crack tip, respectively. Thus, the partial dislocations with $b = a_0/6\langle 112\rangle$ in the {111} plane can be emitted from crack tip due to the addition of Re.

Dislocation emission may be related to kink formation. In Section 3.2.3, it was shown that kink pairs appear near the single Re atom in the (111)[$\bar{1}\bar{1}$2], (0$\bar{1}$1)[100], and ($\bar{1}$10)[$\bar{1}\bar{1}$2] crack systems. Stronger pinning of Re makes the formation of both kinks and dislocations easy. Pinning makes dislocation formation easy because it results in the competition between cleavage and dislocation emission at the crack tip, since pinning makes cleavage difficult.

Besides, at higher temperatures, it is observed in MD simulations that the nucleation of dislocations become easier, and the ductility is enhanced. The simulation results at 300, 500, 700, and 900 K are listed in Table 3. From Table 3, it can be seen that no dislocations nucleation take place for the five crack systems (without Re addition) at 5 K, however, dislocations nucleation appear for the (111)[$\bar{1}\bar{1}$2] and ($\bar{1}$10)[$\bar{1}\bar{1}$2] crack systems when temperature increases to 300 K. When temperature increases to 900 K, dislocations nucleation appear for all the five crack systems. This means the ductility is enhanced when temperature increases. In addition, the ductility of (010)[101] and (100)[010] crack systems is found to be lowest for all the five crack systems, and dislocations nucleation appear difficultly even at higher temperatures. Recalling the discussion in Section 3.2.3 that the kink pairs do not appear in (010)[101] and (100)[010] crack systems, kink and dislocation nucleation should be related.

3.3.5. Influence of Re concentration on fracture stress

The fracture stress (σ_{IC}^+) can be estimated from the following equation:

$$\sigma_{IC}^+ \approx K_{IC}^+/\sqrt{a} \tag{5}$$

where a is the crack length.

The theoretical Griffith stress intensity factor (K_{th}^G) can be calculated from [12]

$$K_{th}^G = (2\gamma/\pi)^{1/2}\{(\beta_{11}\beta_{22}/2)^{1/2}[(\beta_{22}/\beta_{11})^{1/2} + (2\beta_{12}+\beta_{66})/2\beta_{11}]^{1/2}\}^{-1/2} \tag{6}$$

where β_{ij} (i, j = 1, 2, 3, 4, 5, 6) is the plane strain compliance coefficient and γ is the surface energy of the crack surface. Here, we take $(2\gamma/\pi)^{1/2}$ as the surface energy term, and $\{(\beta_{11}\beta_{22}/2)^{1/2}[(\beta_{22}/\beta_{11})^{1/2} + (2\beta_{12} + \beta_{66})/2\beta_{11}]^{1/2}\}^{-1/2}$ as the anisotropic elasticity term.

The fracture stress (σ_{IC}^+) can be calculated from Eqs. (5) and (6) using the values of K_{IC}^+/K_{th}^G from the MD results. It is can be seen from Eqs. (5) and (6) that σ_{IC}^+ is mainly determined by the surface energy term and the anisotropic elasticity term since the lattice-trapping range is small.

Table 4 lists the calculation results for σ_{IC}^+. Table 5 lists the calculation results for the surface energy term, the anisotropic elasticity term, K_{th}^G, K_{IC}^+/K_{th}^G, and σ_{IC}^+, without the addition of Re in the five crack systems. Table 6 lists the calculation results for the surface energy term, the anisotropic elasticity term, K_{th}^G, K_{IC}^+/K_{th}^G, and σ_{IC}^+, with Re addition in the (010)[101] crack system.

From Table 4, it can be seen that the largest and smallest fracture stresses occur in the ($\bar{1}$10)[$\bar{1}\bar{1}$2] and (100)[010] crack systems respectively, without the addition of Re. The reason that the largest σ_{IC}^+ occurs in the ($\bar{1}$10)[$\bar{1}\bar{1}$2] crack system (without Re addition) is that the surface energy term for the ($\bar{1}$10)[$\bar{1}\bar{1}$2] crack system is largest in the five crack systems (Table 5). Meanwhile, it is noticed that the surface energy term for the (0$\bar{1}$1)[100] crack system is also largest in the five crack systems, but σ_{IC}^+ for the (0$\bar{1}$1)[100] crack system is not largest in the five crack systems. This is because the anisotropic elasticity term for the (0$\bar{1}$1)[100] crack system is smaller than that for the ($\bar{1}$10)[$\bar{1}\bar{1}$2] crack system. This indicates that the different anisotropic structure can lead to the different σ_{IC}^+ for ($\bar{1}$10)[$\bar{1}\bar{1}$2] and (0$\bar{1}$1)[100] crack systems, and the direction of crack advance can also influence σ_{IC}^+, though the ($\bar{1}$10)[$\bar{1}\bar{1}$2] and (0$\bar{1}$1)[100] crack systems have the similar {110} crack surface. Thus, the structure factor (namely, the different anisotropic structures) in the different crack systems can determine σ_{IC}^+ without Re addition.

On the other hand, the reason that the smallest σ_{IC}^+ occurs in the (100)[010] crack system (without Re addition) is that the anisotropic elasticity term for the (100)[010] crack system is smallest in the five crack systems, although the surface energy term for the (100)[010] crack system is not smallest in the five crack systems.

Table 3
Appearance or non-appearance of dislocations at different temperatures for the five crack systems.

Crack orientation	5 K			300 K			500 K			700 K			900 K		
	No Re	3% Re	6% Re	No Re	3% Re	6% Re	No Re	3% Re	6% Re	No Re	3% Re	6% Re	No Re	3% Re	6% Re
(010)[101]	–	–	–	–	–	–	–	–	D	–	D	D	D	D	D
(111)[$\bar{1}\bar{1}$2]	–	D	D	D	D	D	D	D	D	D	D	D	D	D	D
(100)[010]	–	–	–	–	–	–	–	–	–	–	–	D	–	–	D
(0$\bar{1}$1)[100]	–	–	D	–	–	D	–	D	D	D	D	D	D	D	D
($\bar{1}$10)[$\bar{1}\bar{1}$2]	–	D	D	D	D	D	D	D	D	D	D	D	D	D	D

Note: "D" or "–" presents whether dislocation emission takes place at the crack tip or not.

Table 4
Fracture stresses (σ_{IC}^{+}, GPa).

Crack orientation	Without Re	1 Re atom	3 at.% Re	6 at.% Re
(010)[101]	7.75	7.75	8.80	10.12
(111)[$\bar{1}\bar{1}$2]	7.69	7.69	D	D
(100)[010]	7.38	7.38	8.47	9.42
(0$\bar{1}$1)[100]	7.68	7.68	8.74	D
($\bar{1}$10)[$\bar{1}\bar{1}$2]	7.80	7.80	D	D

Note: "D" indicates that dislocation emission takes place at the crack tip.

Table 5
The surface energy term, the anisotropic elasticity term, K_{th}^{G}, K_{IC}^{+}/K_{th}^{G}, and σ_{IC}^{+}, without the addition of Re in the five crack systems.

Crack orientation	$(2\gamma/\pi)^{1/2}$ (J/m^2)	AE ($\times 10^5$ Pa$^{1/2}$)	K_{th}^{G} ($\times 10^5$ N/m$^{3/2}$)	$\frac{K_{IC}^{+}}{K_{th}^{G}}$	σ_{IC}^{+} (GPa)
(010)[101]	1.0069	4.807	4.84	1.01	7.75
(111)[$\bar{1}\bar{1}$2]	0.9770	4.871	4.76	1.02	7.69
(100)[010]	1.0069	4.576	4.61	1.01	7.38
(0$\bar{1}$1)[100]	1.0385	4.576	4.75	1.02	7.68
($\bar{1}$10)[$\bar{1}\bar{1}$2]	1.0385	4.690	4.87	1.01	7.80

Note: "AE" represents the anisotropic elasticity term described in Eq. (6).

Table 6
The surface energy term, the anisotropic elasticity term, K_{th}^{G}, K_{IC}^{+}/K_{th}^{G}, and σ_{IC}^{+}, without and with the Re addition in the (010)[101] crack system.

	$(2\gamma/\pi)^{1/2}$ (J/m^2)	AE ($\times 10^5$ Pa$^{1/2}$)	K_{th}^{G} ($\times 10^5$ N/m$^{3/2}$)	$\frac{K_{IC}^{+}}{K_{th}^{G}}$	σ_{IC}^{+} (GPa)
Without Re	1.0069	4.807	4.84	1.01	7.75
3 at.% Re	1.0133	4.806	4.87	1.14	8.80
6 at.% Re	1.0261	4.824	4.95	1.29	10.12

Note: "AE" represents the anisotropic elasticity term described in Eq. (6).

When 3 at.% or 6 at.% Re is added, σ_{IC}^{+} usually increases by at least 10%, and the smallest σ_{IC}^{+} still occurs in the (100)[010] crack system, but the largest σ_{IC}^{+} occurs in the (010)[101] crack system instead of ($\bar{1}$10)[$\bar{1}\bar{1}$2] crack system (Table 4). With the addition of 3 at.% or 6 at.% Re, the dislocation appears in the ($\bar{1}$10)[$\bar{1}\bar{1}$2] crack system and the ($\bar{1}$10)[$\bar{1}\bar{1}$2] crack becomes blunt, and σ_{IC}^{+} is meaningless for the blunt crack. Thus instead, σ_{IC}^{+} for the (010)[101] crack system becomes largest. This means that the chemical factor (the surface energy term) by Re addition can also have a big effect on σ_{IC}^{+}, comparing to the structure factor. From Table 6, it can be seen that almost all values of the surface energy term, the anisotropic elasticity term, K_{th}^{G}, K_{IC}^{+}/K_{th}^{G}, and σ_{IC}^{+} increase with the addition of Re, and the increase magnitudes of both the surface energy term and anisotropic elasticity term reach the same level. This indicates that the chemical factor is also important to σ_{IC}^{+}, comparing to the structure factor.

4. Conclusions

In the present work, the influence of Re on the lattice trapping and fracture stress of brittle cracks in Ni is investigated. The following conclusions are drawn.

(1) Without Re addition, the true Griffith load in the MD simulation is very close to the theoretical Griffith load, and $K_{IC}^{-}/K_{th}^{G} \approx 0.98 \sim 1.00$; $K_{IC}^{+}/K_{th}^{G} \approx 1.01 \sim 1.02$.
(2) The lattice-trapping range for the five different crack orientations studied is small ($K_{IC}^{+}/K_{IC}^{-} - 1 \approx 0.03$), regardless of the addition of Re. This implies that the Re–Ni interatomic interaction also has long-range characteristics.
(3) A single Re atom has no effect on both K_{IC}^{-} and K_{IC}^{+}. With the addition of 3 at.% and 6 at.% Re, both K_{IC}^{-} and K_{IC}^{+} increase significantly, which means that Re–Ni atomic interaction can prevent the breaking of atomic bonds and can heal cracks.
(4) The largest and smallest σ_{IC}^{+} occur in the ($\bar{1}$10)[$\bar{1}\bar{1}$2] and (100)[010] crack systems respectively, without the addition of Re. The surface energy and the anisotropic structure can lead to the different σ_{IC}^{+}; with the addition of 3 at.% or 6 at.% Re, σ_{IC}^{+} usually increases by at least 10%, and the largest and smallest σ_{IC}^{+} values occur in the (010)[101] and (100)[010] crack systems, respectively. The chemical factor by Re addition can also have a big effect on σ_{IC}^{+}.
(5) $R < 5$ Å in dilute Ni (Re) solid solutions; $R > 17$ Å in concentrated Ni (Re) solid solutions. $K_{IC}^{\pm}$ is proportional to R.
(6) The appearance of kink at crack front is caused by stronger pinning of Re, and does not affect S and R. In addition, S does not affect R.

Acknowledgments

The authors would like to acknowledge the support of the National Basic Research Program of China (Grant No. 2011CB606402) and the National Natural Science Foundation of China (Grant No. 51071091). Simulations were performed using the "Explorer 100" cluster system at the Tsinghua National Laboratory for Information Science and Technology, Beijing, China.

References

[1] R. Thomson, C. Hsieh, V. Rana, J. Appl. Phys. 42 (1971) 3154.
[2] P. Gumbsch, R.M. Cannon, MRS Bull. 25 (2000) 15.
[3] P. Gumbsch, J. Mater. Res. 10 (1995) 2897.
[4] Majid Karimi, Tom Roarty, Theodore Kaplan, Mater. Sci. Eng. 14 (2006) 1409–1420.
[5] J.E. Sinclair, Philos. Mag. 31 (1975) 647.
[6] Sulin Zhang, Ting Zhu, Ted Belytschko, Phys. Rev. B 76 (2007) 094114.
[7] Ting Zhu, Ju Li, Sidney Yip, Proc. R. Soc. A 462 (2006) 1741–1761.
[8] J.E.R. Fuller, R. Thomson, New York: Pergamon 3 (1977) 387.
[9] G. Schoeck, W. Pichl, Phys. Status Solidi A 118 (1990) 109.
[10] Rubén Pérez, Peter Gumbsch, Phys. Rev. Lett. 84 (2000) 5347.
[11] J.P. Du, C.Y. Wang, T. Yu, Modell. Simul. Mater. Sci. Eng. 21 (2013) 015007.

[12] G.C. Sih, H. Liebowitz, Mathematical theories of brittle facture, In: Fracture: An Advanced Treatise, vol. 2, Academic Press, New York, 1968 (Chapter 2).
[13] P. Lazar, R. Podloucky, Phys. Rev. B 78 (2008) 104114.
[14] J.C.H. Spence, Y.M. Huang, O. Sankey, Acta Metall. Mater. 41 (1993) 2815–2824.
[15] Y.F. Guo, Y.S. Wang, W.P. Wu, D.L. Zhao, Acta Mater. 55 (2007) 3891–3897.
[16] M.P. Allen, D.J. Tildesley, Computer Simulation of Liquids, Oxford University Press, New York, 1987. p. 83.
[17] J. Riffkin, Center for Simulation, University of Connecticut, CT. <http://www.ims.uconn.edu/centers/simul/>.
[18] M.S. Daw, M.I. Baskes, Phys. Rev. Lett. 50 (1983) 1285.
[19] M.S. Daw, M.I. Baskes, Phys. Rev. B 29 (1984) 6443.
[20] Z.G. Liu, C.Y. Wang, T. Yu, Modell. Simul. Mater. Sci. Eng. 21 (2013) 045009.
[21] C. Kittel, Introduction to Solid State Physics, Wiley, New York, 1976.
[22] S.G. Lekhnitskii, Theory of an Anisotropic Body, Holden-Day, San Francisco, 1963. p. 109.
[23] P.A. Gordon, T. Neeraj, Acta Mater. 57 (2009) 3091.
[24] S.Y. Wang, C.Y. Wang, J.H. Sun, W.H. Duan, D.L. Zhao, Phys. Rev. B 65 (2001) 035101.
[25] F.H. Wang, C.Y. Wang, Phys. Rev. B 57 (1998) 289–295.
[26] D. Guenzburger, D.E. Ellis, Phys. Rev. B 45 (1992) 285.
[27] D.E. Ellis, G.A. Benesh, E. Byrom, Phys. Rev. B 16 (1977) 3308.
[28] G. Kresse, J. Furthmuller, Comput. Mater. Sci. 6 (1996) 15.
[29] G. Kresse, J. Furthmuller, Phys. ReV. B 54 (1996) 11169.